Synthesis, Characterization, and DFT Studies of Thione and Selone Cu(I) Complexes with Variable Coordination Geometries

Martin M. Kimani, Craig A. Bayse, and Julia L. Brumaghim*

SUPPLEMENTARY INFORMATION

Crystal packing diagrams for $Cu_4(\mu\text{-dmise})_4(\mu\text{-I})_2I_2$ (**1**) and $CuI(dmit)_2$ (**3a**) (Fig S1-S2), XRD powder patterns for copper complexes **1**, **2**, **3**, **4**, **5**, **6**, **7**, and **8** (Fig S3-S12), cyclic voltammograms for all copper complexes (Fig S13), and DPV voltammograms for tetrameric complexes **1** and **6** (Figs. S14-S15).

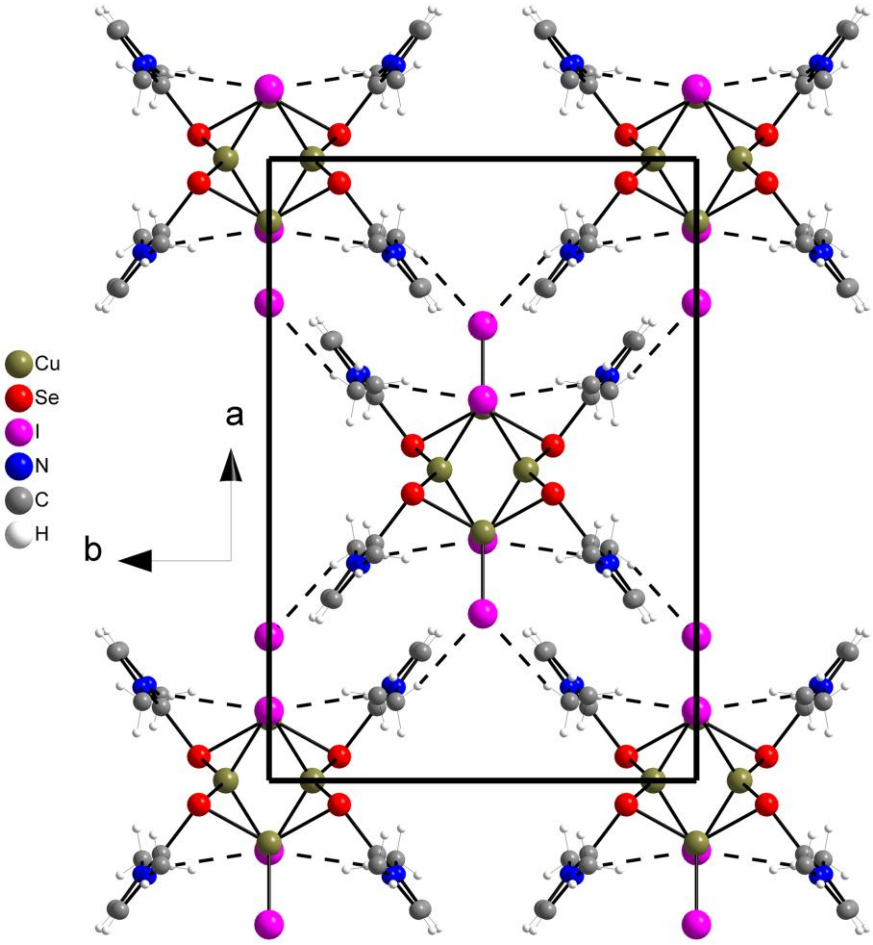

Figure S1. Crystal packing diagram of $Cu_4(\mu\text{-dmise})_4(\mu\text{-I})_2I_2$ (**1**) along the *c*-axis depicting short contact interactions between Se and H atoms.

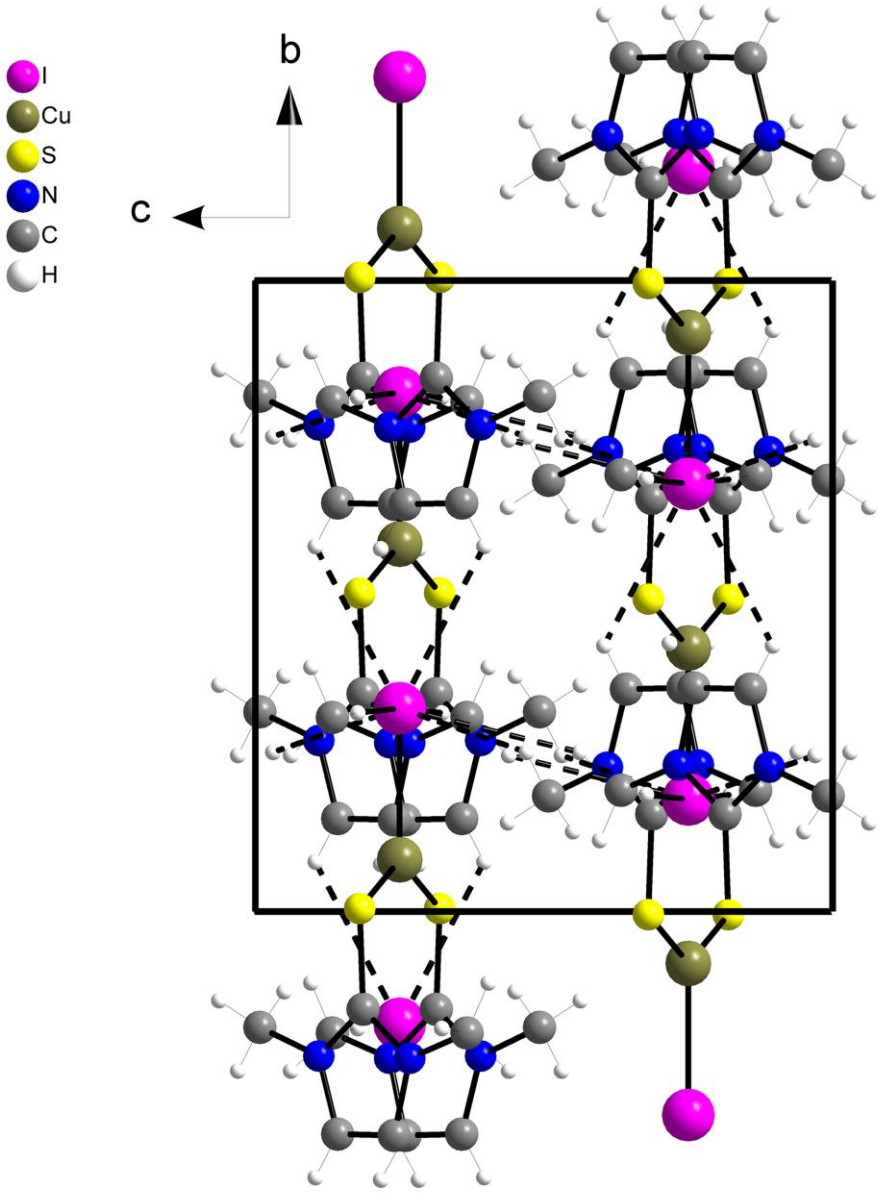

Figure S2. Crystal packing diagram of $CuI(dmit)_2$ (**3a**) along the *a*-axis depicting short contact interactions between Se and H atoms.

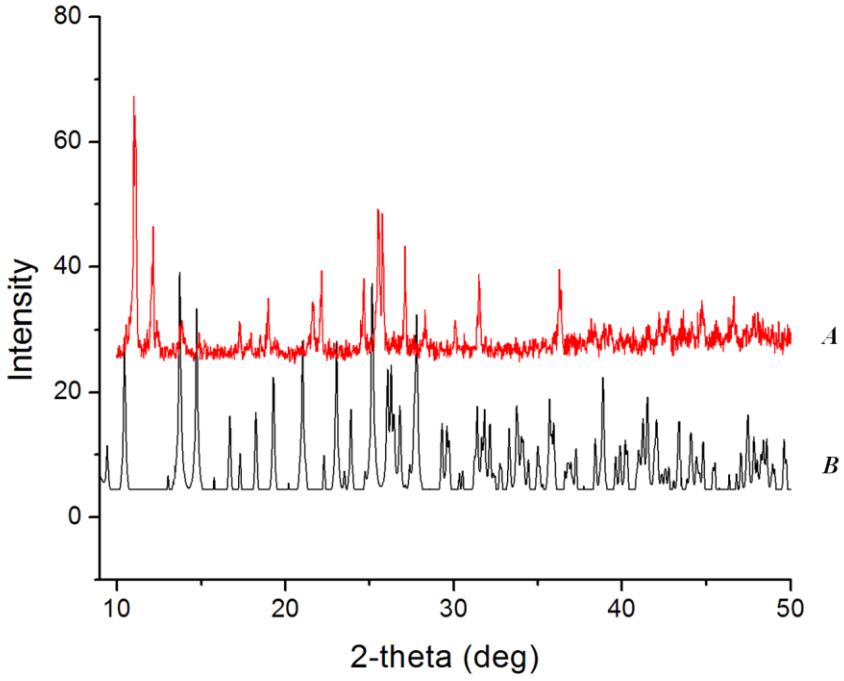

Figure S3. Powder X-ray diffraction pattern of A) $Cu_4(\mu\text{-dmise})_4(\mu\text{-I})_2I_2$ (**1**), vs. simulated powder pattern B) for $Cu_4(\mu\text{-dmise})_4(\mu\text{-I})_2I_2$ (**1**).

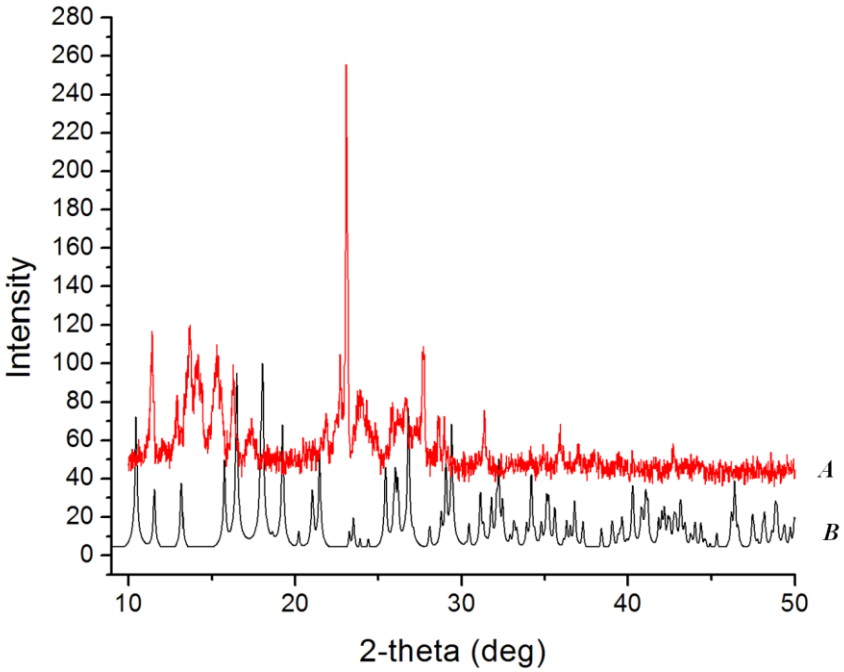

Figure S4. Powder X-ray diffraction pattern for **A**) $CuI(dmise)_2$ (**2**), vs. simulated powder pattern for B) $CuI(dmise)_2$ (**2**).

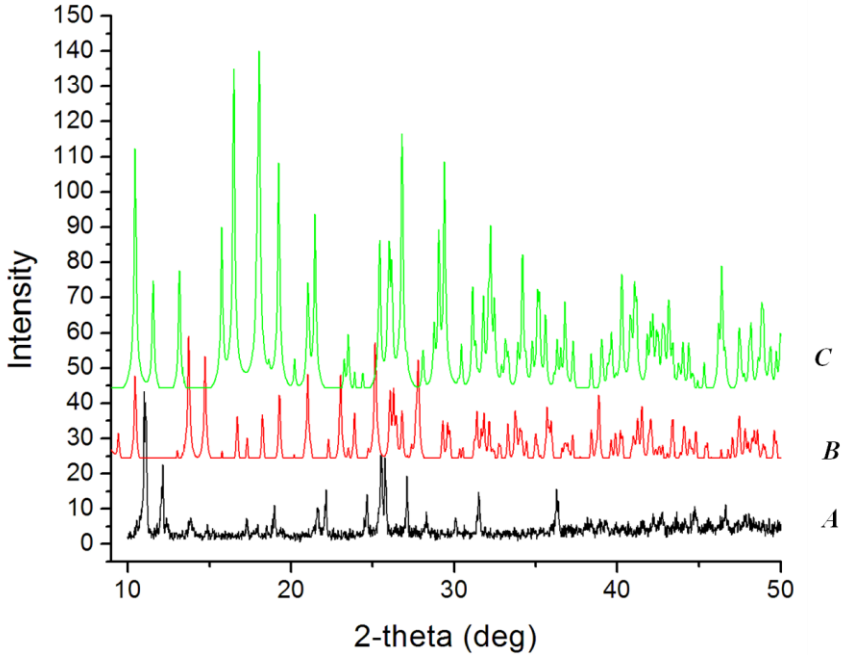

Figure S5. Experimental powder X-ray diffraction pattern of A) $Cu_4(\mu\text{-dmise})_4(\mu\text{-I})_2I_2$ (**1**), vs. simulated powder pattern for B) $Cu_4(\mu\text{-dmise})_4(\mu\text{-I})_2I_2$ (**1**), and C) $CuI(dmise)_2$ (**2**).

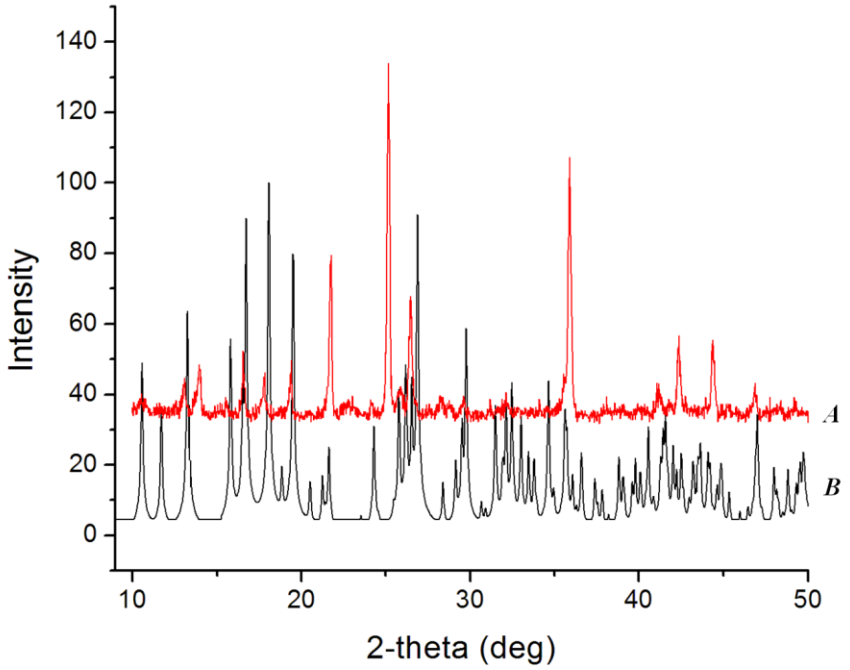

Figure S6. Powder X-ray diffraction pattern for A) $CuI(dmit)_2$ (**3b**) vs. simulated powder pattern for B) $CuI(dmit)_2$ (**3b**).

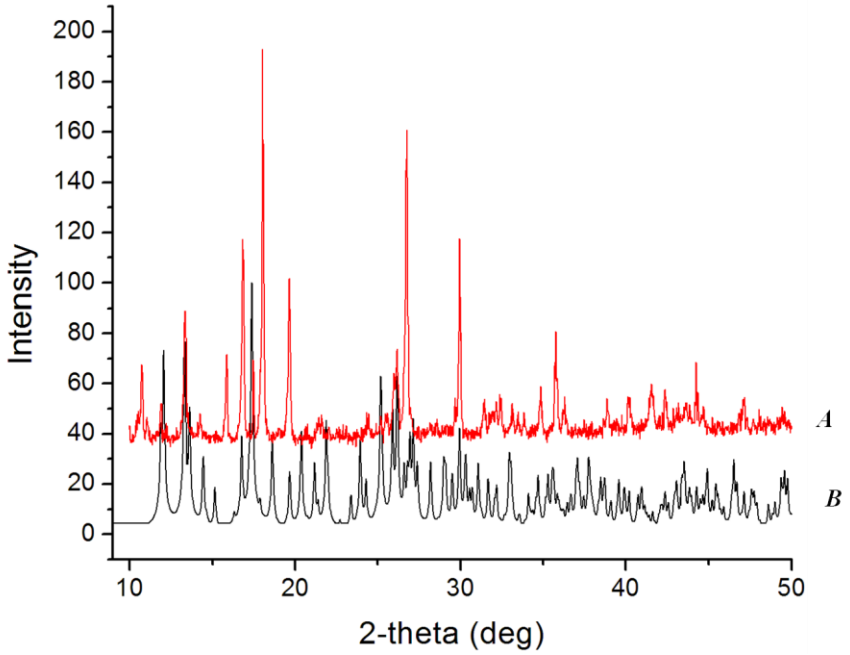

Figure S7. Powder X-ray diffraction pattern for **A**) $CuI(dmit)_2$ (**3a**) vs. simulated powder pattern for **B**) $CuI(dmit)_2$ (**3a**).

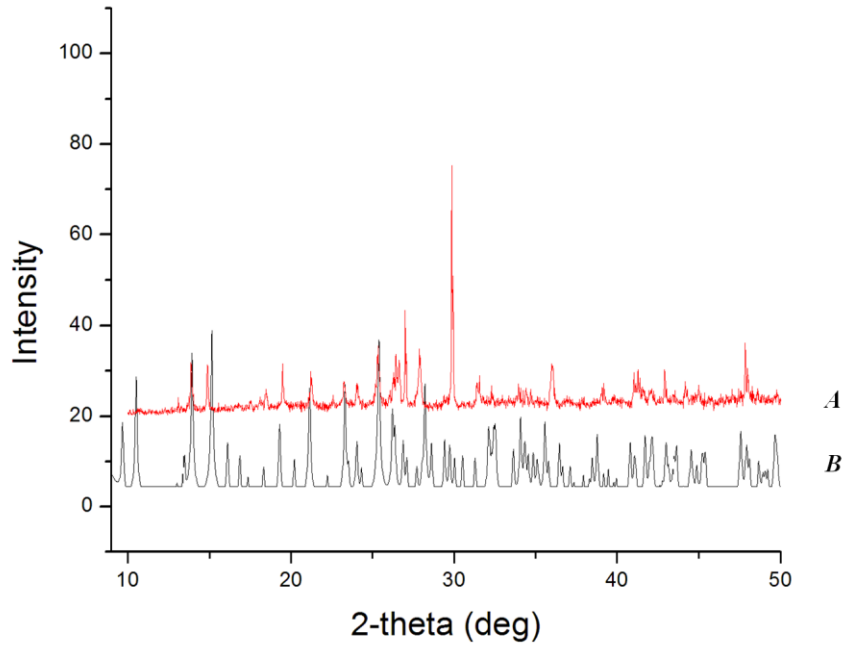

Figure S8. Experimental powder x-ray diffraction pattern of A) $Cu_4(\mu\text{-dmise})_4(\mu\text{-Br})_2Br_2$ (**6**) vs. simulated powder pattern B) for $Cu_4(\mu\text{-dmise})_4(\mu\text{-Br})_2Br_2$ (**6**).

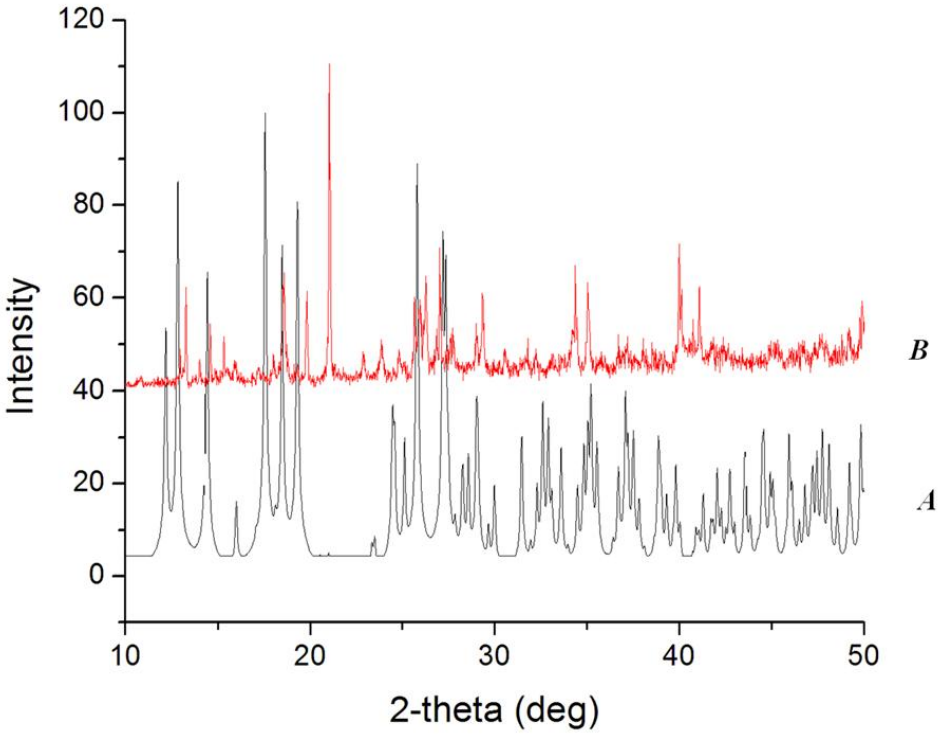

Figure S9. Experimental powder x-ray diffraction pattern of B) $CuBr(dmise)_2$ (**8**), vs. simulated powder pattern A) for $CuBr(dmise)_2$ (**8**).

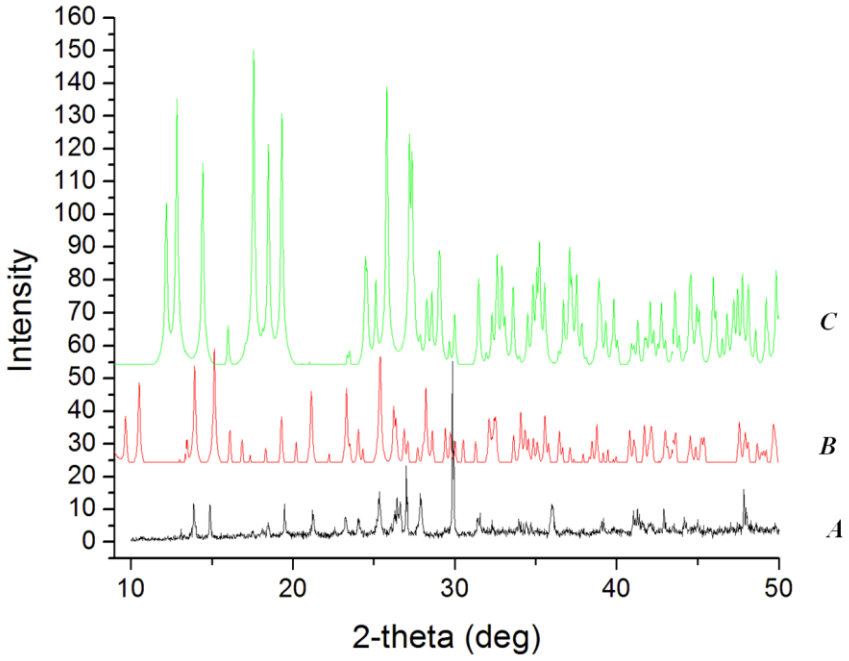

Figure S10. Experimental powder x-ray diffraction pattern of A) $Cu_4(\mu\text{-dmise})_4(\mu\text{-Br})_2Br_2$ (**6**), vs. simulated powder pattern B) for $Cu_4(\mu\text{-dmise})_4(\mu\text{-Br})_2Br_2$ (**6**), and C) $CuBr(dmise)_2$ (**8**).

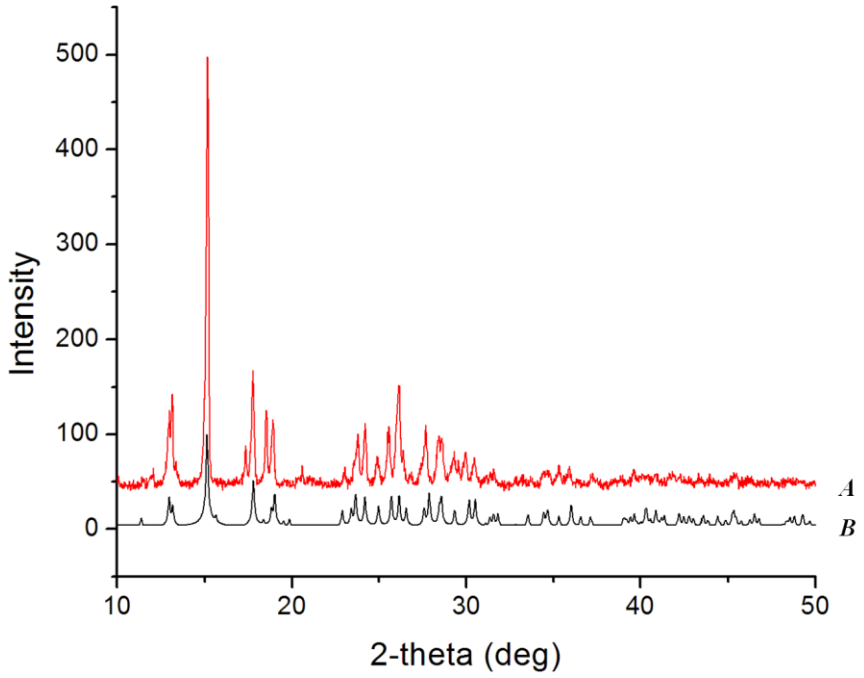

Figure S11. Experimental powder X-ray diffraction pattern of A) $CuCl(dmit)_2$ (**4**), vs. simulated powder pattern for B) $CuCl(dmit)_2$ (**4**).

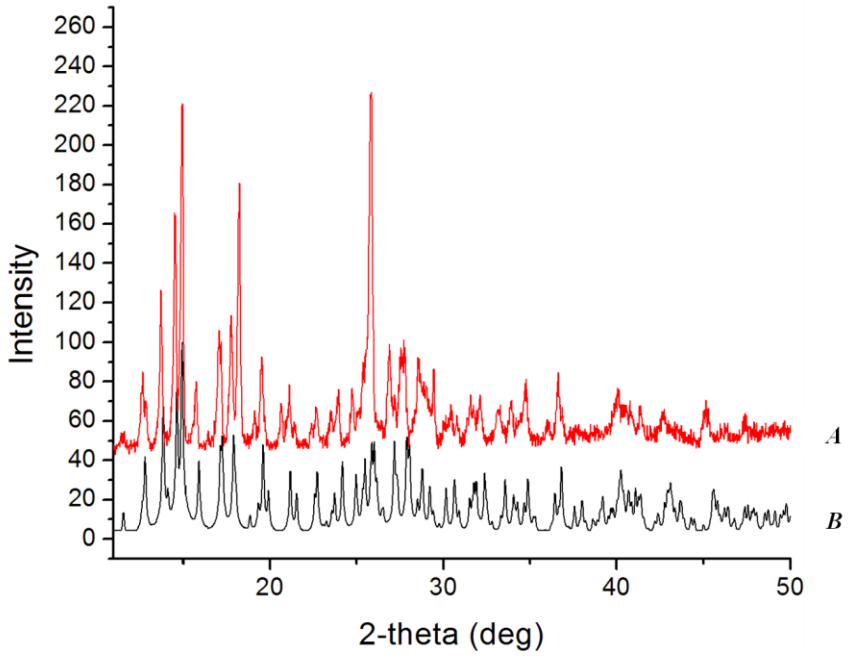

Figure S12. Experimental powder X-ray diffraction pattern of A) $CuCl(dmise)_2$ (**5**), vs. simulated powder pattern for B) $CuCl(dmise)_2$ (**5**).

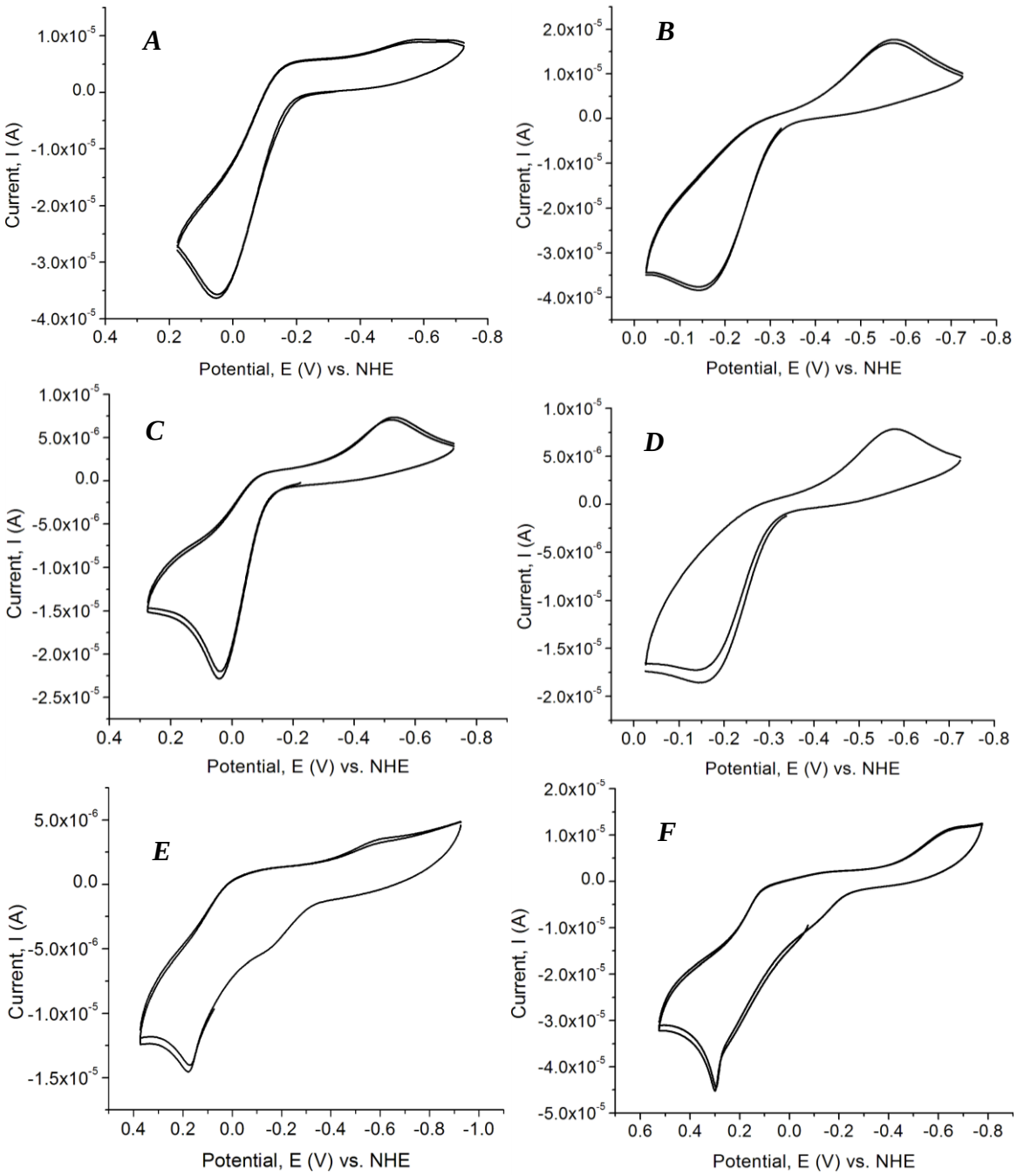

Figure S13. Cyclic voltammetry scans for A) $CuCl(dmit)_2$, B) $CuCl(dmise)_2$, C) $CuBr(dmit)_2$, D) $CuBr(dmise)_2$, E) $CuI(dmit)_2$ **3a**, F) $CuI(dmit)_2$ **3b**. All data collected with 10^{-3} M complex in acetonitrile.

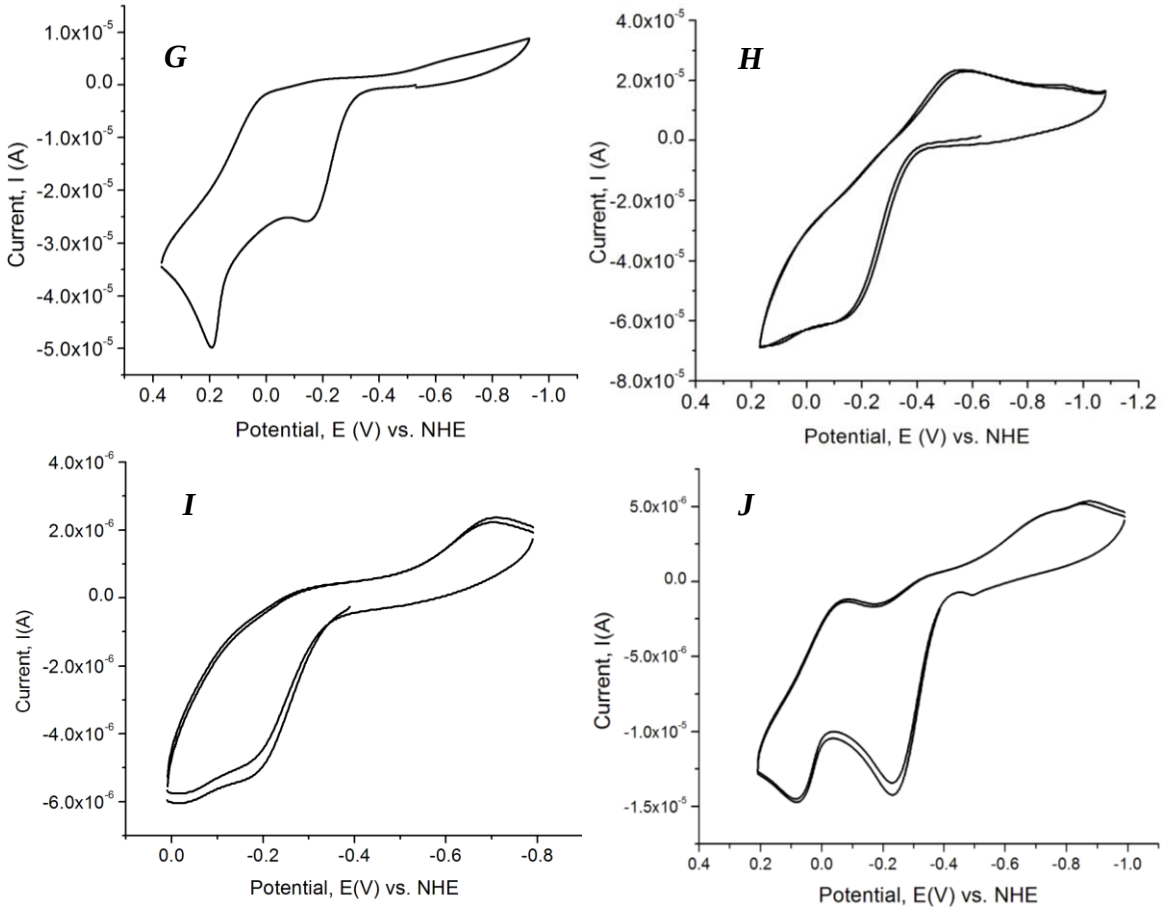

Figure S13 (continued). Cyclic voltammetry scans for G) mixed *trans*- and *cis*-CuI(dmit)$_2$ (**3a** and **3b**), H) CuI(dmise)$_2$, I) Cu$_4$(μ-dmise)$_4$(μ-Br)$_2$Br$_2$, J) Cu$_4$(μ-dmise)$_4$(μ-I)$_2$I$_2$. All data collected with 10^{-3} M complex in acetonitrile.

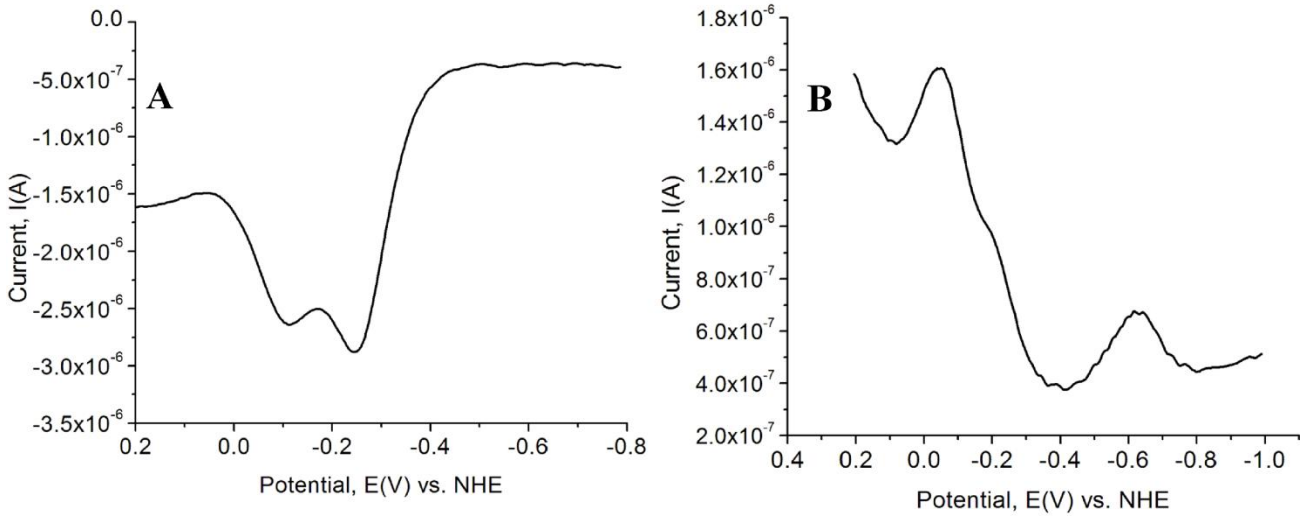

Figure S14. Differential pulse voltammograms: A) positive scan of Cu$_4$(μ$_4$-dmise)(μ-Br)$_2$Br$_2$ (**6**); B) negative scan of Cu$_4$(μ$_4$-dmise)(μ-Br)$_2$Br$_2$ (**6**). DPV data were collected at a concentration of 1 mM in acetonitrile.

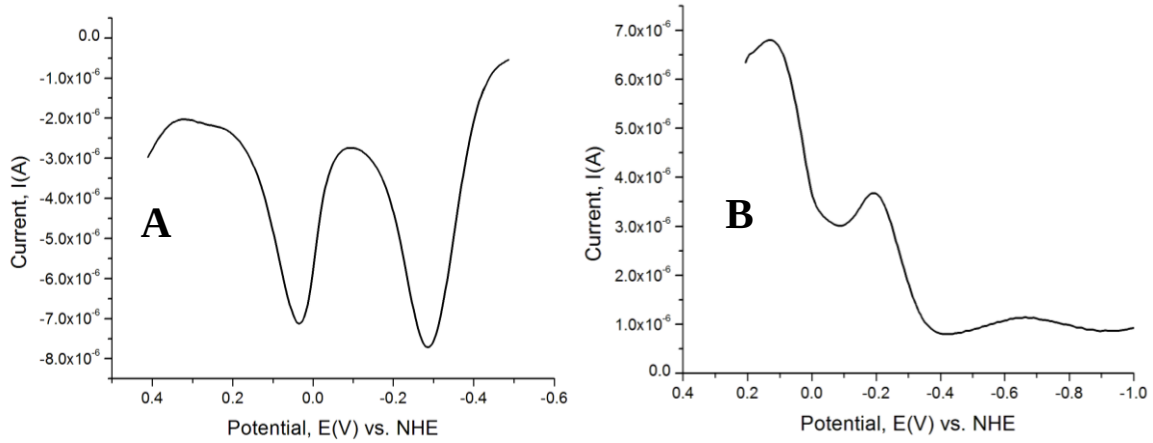

Figure S15. Differential pulse voltammograms: A) positive scan of $Cu_4(\mu_4\text{-dmise})(\mu\text{-I})_2I_2$ (**1**); B) negative scan of $Cu_4(\mu_4\text{-dmise})(\mu\text{-I})_2I_2$ (**1**). DPV data were collected at a concentration of 1 mM in acetonitrile.